Article

Graphene-Alumina Nanocomposites with Improved Mechanical Properties for Biomedical Applications

Jian Liu, Yang Yang, Hany Hasssinin, Neeraj Jumbu, Sunan Deng, Qian Zuo, and K. Jiang

ACS Appl. Mater. Interfaces, **Just Accepted Manuscript** • DOI: 10.1021/acsami.5b10424 • Publication Date (Web): 24 Dec 2015

Graphene-Alumina Nanocomposites with Improved Mechanical Properties for Biomedical Applications

Jian Liu[a] *, Yang Yang[b], Hany Hasssinin[c], Neeraj Jumbu[d], Sunan Deng[b], Qian Zuo[a], Kyle Jiang[b,e] *

[a]*School of Manufacturing Science and Engineering, Sichuan University, Chengdu, China, 610065.*

[b]*Biomedical Engineering and Micro/Nanotechnology Research Centre, School of Mechanical Engineering, University of Birmingham, Birmingham,B15 2TT, UK.*

[c]*School of Mechanical and Automotive Engineering, Kingston University, London, KT1 2EE, UK.*

[d]*School of Chemical Engineering, University of Birmingham, Birmingham,B15 2TT, UK.*

[e]*School of Materials Sciences and Engineering, Taiyuan University of Science and Technology, Wanbailin District, 030024, Taiyuan, China*

Abstract: The paper presents a study on graphene platelet (GPL)-reinforced alumina (Al_2O_3) ceramic composites and the relationships between the loading of GPL and both mechanical properties and in-vitro biocompatibility. Al_2O_3 powders with different GPL contents were prepared and sintered using a gas protected pressure-less furnace. The examination of the results shows the density of the composites varying from 99.2% to 95.6% with the loading of GPL from 0.75 to 1.48 vol%. Raman studies show that moderate agglomerations of GPLs

* Corresponding authors,liujian@scu.edu.cn and k.jiang@bham.ac.uk.

Yang Yang has contributed equally to the work as the first author.

occur during the ball milling process and graphitic defects were produced during the high temperature processing. Mechanical properties of the Al_2O_3 matrix are significantly improved by adding GPLs. A maximum increase of approximately 60% in flexural strength and 70% in fracture toughness are achieved by introducing 0.75 vol% GPLs. In the biocompatibility tests it was found that cells directly seeding on top of GPL/Al_2O_3 samples showed better initial attachment (3 hours after seeding) and viability (3 days after incubation) than the monolithic Al_2O_3, indicating that the GPL/Al_2O_3 composites have comparable or more favorable biocompatibility. The excellent mechanical and biomedical properties of the GPL/Al_2O_3 composites may enable them to be applied to a wide range of engineering and biomedical applications.

Keywords: Graphene platelets, Ceramic matrix composites; Mechanical properties; In-vitro Biocompatibility; Pressure-less sintering.

1. Introduction

Ceramics have been applied as biomaterials for many decades due to their superior mechanical and biocompatible properties. One particular such application is ceramic heads of hip joint prostheses [1]. In addition, ceramics have also been used clinically in the femoral components of knee joint prostheses and ankle joint prostheses [2]. In other medical fields, ceramics are used as artificial bone to repair cranial and orbital bone defects and as dental and cochlear implants [3-7]. Despite the widespread usage, further applications of ceramics are seriously limited by their intrinsic brittleness. In the last few decades, much effort has been paid to improve the toughness of the ceramics using micro- and nano-structures as reinforcements. These methods have the similar aim of providing additional intrinsic grain boundaries or extrinsic interfaces that prohibit dislocation-movement and long paths of crack

propagation [8-10].

Graphene has received enormous attention globally in recent years. Its excellent electrical and mechanical properties make it suitable for many applications [11]. Compared to monolayer graphene, graphene platelets (GPLs) are stacked graphene with thickness of up to approximately 100 nm [12]. It is reported that the Young's modulus of GPLs with thickness of 2-8 nm is approximately 0.5 TPa [13], higher than many ceramics. Analogous to ceramic composites reinforced with micro-fibres, incorporation of GPLs into ceramic matrices is expected to lead to considerable improvement in strength and toughness. However, the effectiveness varies in reported literature. It is suggested that three factors need to be carefully addressed in the fabrication process in order to utilize graphene's full potential to improve the mechanical properties of the ceramics [12, 14-15]. They are (i): homogeneous dispersion of GPLs in matrices to prevent GPLs agglomeration caused by Van der Waals forces; (ii) full densification of the composites; (3) retention of the graphitic structure during the high temperature process. Since the agglomeration of GPLs is the source of cracks and cause of the degradation of the mechanical properties, the preparation routes for producing GPL/ceramic composite powders are critical to ensure the excellent performance of the sintered composites. At present, a variety of the preparation methods such as conventional powder mixing, colloidal mixing and molecular mixing have been adopted to form a homogenous distribution of GPLs in the ceramic powder. Among them, powder mixing is considered the most efficient way and easy to scale up for volume production. In particular, it has been proved that when Dimethylformamide or N-methylformamide (NMP) is utilized as solvent, a homogenous dispersion of GPLs with reasonably small thickness in the powder mixtures can be obtained. Another vital factor is to best retain the GPLs during the densification of composites. This way, good bonding between the GPLs and matrices can be created and high stiffness of GPLs can be preserved, which facilitates load transfer at the

interface between the GPLs and matrix and provide good reinforcing and toughening efficiencies.

Currently, many studies have been reported on GPL/polymer composites with enhanced mechanical and electrical properties while only few reports can be found to explore the GPL/ceramic composites. It is partly due to the fact that it is relatively more difficult to acquire sintered ceramic components than polymer one. Several researchers have made the attempts. Walker et al. employed aqueous colloidal processing methods to obtain homogeneous dispersions of GPLs and silicon nitride (Si_3N_4) ceramic particles which were densified using spark plasma sintering (SPS) [16]. The measured fracture toughness of 6.6 MPa $m^{1/2}$ for the composite with 1.5wt% of GPLs was 136% higher than that of monolithic Si_3N_4. Dusza et al. prepared the GPL-reinforced Si_3N_4 composite containing 1 wt% GPLs using hot isostatic pressing and reported a 44% increase in fracture toughness over pure Si_3N_4 [17]. Liu et al. employed the SPS to fabricate the GPL/zirconia (ZrO_2)-toughened Al_2O_3 composite with addition of 0.81vol% GPLs and found an about 40% increase in fracture toughness [12]. More recently, Yadhukulak-rishnan et al. fabricated GPL-reinforced zirconium diboride composites at a high sintering temperature using SPS and investigated the effect of GPL content on mechanical properties of the composites[18] and found an about 110% increase in fracture toughness of the composite with addition of 6 vol% GPLs. Nieto et al. used SPS to consolidate GPL/tantalum carbide (TaC) ceramic composites and found the fracture toughness of the GPL/TaC composite containing 5 vol% GPLs was 99% higher than that of pure TaC ceramic [19]. In fabrication of GPL/ceramic composites, advanced consolidation techniques such as SPS, hot isostatic pressing and hot pressing are usually preferred since the sintering densification process can be realized in a short time and a vacuum or inert environmentas well as high pressure can be maintained to protect the GPLs.

In the exploration of graphene composites for biomedical applications, a few studies indicate the cytotoxicity of graphene is dose-dependent and caused by oxidative stress generated incontact with graphene [20-21] while others showing enhanced adhesion and spread of the cells [22]. The contradictory results might be associated with the types of cells and GPLs used in the experiments. Lahiri et al. prepared the GPL/ultrahigh molecular weight polyethylene (UHMWPE) composites for orthopedic implants and found that the viability of osteoblasts deteriorates up to 86% on the surface of the UHMWPE composite reinforced by 1.0 wt.% GPLs [23]. Zhang et.al fabricated GPL/hydroxyapatite (HA) composites and reported that an addition of 1 wt% GPLs led to significant improvement of osteoblast adhesion [22].

Very few reports can be found on pressure-less sintering of GPL/ceramic composites and the biocompatibility of GPL/ceramic composites and this study is set out to investigate them. Pressure-less sintering of GPL/Al_2O_3 composites was carried out in a gas protected tube furnace and mechanical properties of the fabricated composites were studied. Raman spectroscopy was used to analyze the structural integrity of the GPLs. Phase composition and grain size of the ceramics were determined by the x-ray diffraction (XRD) and scanning electron microscopy (SEM) respectively. The effects of the GPL on the in-vitro biocompatible properties of the GPL/Al_2O_3 composite materials were investigated using cell adhesion and 3-(4,5)-dimethylthiahiazo (-z-y1)-3,5-di- phenytetrazoliumromide (MTT) tests. The role of the GPLs and their contributions towards the mechanical response and in-vitro biocompatibility of the GPL/Al_2O_3 composite were analysed and discussed.

2. Experimental procedure

2.1 Starting materials

α-Al_2O_3 powder (99.85%, 150 nm, Inframat Advanced Materials, Farmington, CT, USA) was used in this study. SEM images of Al_2O_3 are presented in Figure 1a. GPLs were procured

from Graphene Industries Ltd, Manchester, UK. SEM images of the obtained GPLs are shown in Figure 1b and 1c. A general approach to produce the GPLs is via rapid thermal expansion/exfoliation of graphite that has been intercalated using sulphuric acid.The resultant platelets are stacks of graphene sheets about 6-8 nm in thickness and 15-25 μm in diameter.

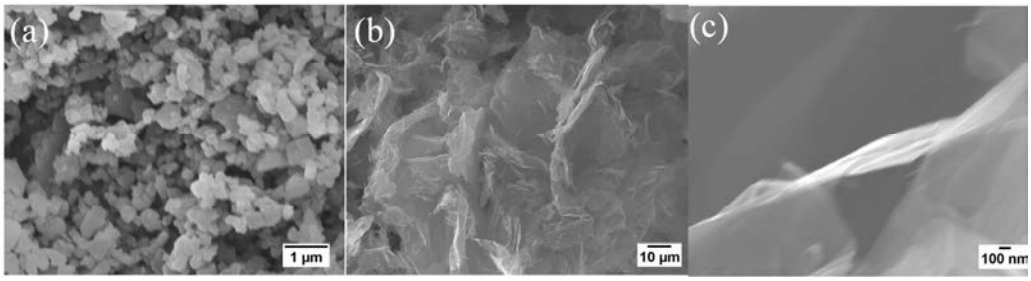

Figure.1 SEM images of Al_2O_3 (a) powders and GPLs (b-c).

2.2 Powder mixture and green compact preparations

GPLs were first dispersed in NMP and sonicated for 40 minutes. Appropriate quantities of Al_2O_3 nanoparticles were added and then the mixture was further sonicated for 10 minutes. This was followed by a ball milling procedure at 100 rpm in a planetary ball mill (PM 100, Retsch, UK) for 2 hours. The milling was carried out in a cylindrical ZrO_2container using ZrO_2 balls under a ball-to-powder weight ratio of 2. The milled slurry mixture was dried at 90 ˚C in an oven for 3 days. The dried powder mixture was ground and sieved using a 140 mesh. Figure S1 shows the SEM images of the powder mixtures. A soft mould was then filled with the dried powders and subsequently underwent cold isostatic pressing to form green compacts.

2.3 Pressure-less sintering

Green compacts with nominal contents of 0, 1.17, 1.85 and 2.75 vol% GPLs were sintered using a tube furnace. Sintering temperature of 1650°C, soaking time of 2.5-3h and forming gas with flowing rate of 8 L/min were used to densify the powder mixtures.

2.4 Mechanical measurements and microstructure characterization

The sintered samples were ground and polished to 0.5μm using silicon carbide papers and diamond suspension. The bulk density of the samples was measured using the Archimedes method with ethanol as the immersion medium. The densities of Al_2O_3 and GPL adopted were 3.97 and 2.1 g m^{-3}. The relative density was calculated by dividing the bulk density with the theoretical density of the powder mixture. Vicker hardness tests were carried out under a 1kg force. Flexural strength and fracture toughness of the sintered samples were obtained using four-point bending tests on an Instron 6025. In the flexural strength tests, specimens of 1.5 × 2× 13 mm were machined. The span length and crosshead speed for the strength tests were 10 mm and 0.05 mm min^{-1}. To avoid stress concentration, all the edges and corners of the specimens were chamfered using SiC grinding papers. The Single-edge V-notch beam method was used to determine the fracture toughness of the sintered samples at room temperature. Specimens of 2 × 3 × 15 mm were machined for toughness measurement. Notches at the centre of the test specimens were cut by a diamond wheel and further sharpened using a razor blade with the aid of diamond paste up to 1 μm. The ratio between the notch depth and specimen thickness was approximately 0.25. Inner and outer spans of 6 mm and 10 mm, as well as a crosshead speed of 0.05 mm/min, were applied in the toughness tests. Five samples were tested for each material. SEM was used to examine fracture surfaces of the ceramics and the polished samples thermally etched. Grain sizes were measured with the aid of the software (UTSHCSA, USA). At least 200 readings were taken to measure the grain sizes of each material. A Raman Microscope (Renishaw InVia Reflex and Witec Alpha 300R) was used to characterise the GPLs in the powder mixtures and sintered samples with the 532 nm laser wavelength excitation. Thermo gravimetric analysis (TGA, NETZSCH (STA 449C)) was carried out to examine the GPL contents within the sintered samples.The sintered samples were crushed, milled and sieved using a 140 mesh to produce powder

mixtures for the TGA. In each test, a powder mixture of 100 mg was placed in an Al_2O_3 crucible and examined in the temperature range between 200 and 800 ℃ in air. 800 ℃ was used as the upper limit in the TGA tests with the consideration that oxidation of GPLs should be completed at this temperature according to references [24-26].

2.5 In-vitro biocompatibility tests

Samples were machined to the disk shape with diameter of 18 mm and thickness of 2 mm for biocompatibility evaluation. All GPL/Al_2O_3 composites and control group (the pure Al_2O_3 ceramic) were supersonically cleaned in deionized water and acetone for 15 minutes separately, to remove any possible surface chemical groups or contaminations during fabrication and mechanical test procedures. Then all samples were sterilized by exposing to ultraviolet light overnight before the biological tests.

All biological reagents were obtained from Sigma Aldrich (Poole UK) unless otherwise stated. MTT assays were conducted to examine a pre-osteoblastic cell line (MC3T3) viability on the sintered samples. MC3T3 cells were thawed from liquid nitrogen stock (at passage number 10), cultured in dulbecco minimum essential medium (DMEM) (Sigma D6546, supplemented with 10% Fetal Bovine Serum, 2% L-glutamine,2.4% 2-[4-(2-Hydroxyethyl)-1-piperazinyl] ethanesulfonic acid (HEPES) buffer and 1% penicillin-streptomycin) and incubated at 37°C in a humidified incubator with 5% CO_2. After reaching 80% confluence, cells were trypsinised, centrifuged and re-suspended. Then cells were seeded onto prepared samples at the density of 50000 cells/cm^2, cultured in an incubator for designed time periods and then washed gently with phosphate buffered saline (PBS) to get rid of floating cells before MTT assay.

10% w/v of MTT solution (5 mg/ml of MTT powder in PBS) was added into each assay. After incubation for 4 hours at 37°C, 1 ml of solvent (0.1 mol/L hydrochloric acid in 2-

propanol) was added into each assay and mixed for 2 minutes to dissolve formazan crystals formed. Formazan solution was pipetted into a 96 well plate. Absorbance data was acquired using a microplate spectrophotometer (Glowmax Multi, Promega Southampton, UK) at 560 nm reference wavelength.

Another set of cell adhesion tests were carried out using bone marrow stem cells (BMSCs). Primary cells were extracted from rat tibia and fibias and then cultured in alpha MEM (supplemented with 10% Fetal Bovine Serum, 2% L-glutamine, 1% penicillin-streptomycin and 2.4% HEPES Buffer) and incubated at 37°C in a humidified incubator with 5% CO_2. BMSCs were detached from cell culture flask and were then seeded onto the prepared samples. Meanwhile, tissue culture plastic and Polydimethylsiloxane (PDMS) substrates were used as positive and negative references respectively. Cells were cultured in an incubator at 37 °C with supplemented Alpha MEM. After 3 days of cell culture, cells were stained with 1ug/ml Calcein and 1ug/ml Propidium Iodide and inspected in florescence microscopes.

3. Results and discussion

3.1 Effects of content of GPLs on the microstructures and mechanical properties of GPL/Al_2O_3 composites.

3.1.1 The content of GPLs within the sintered composites.

The results of TGA tests are shown in Figure S2. It is found that the sintered GPL/Al_2O_3 composites contain 0.4, 0.69 and 0.79 wt% GPLs respectively and the corresponding volume percentages of GPLs in the sintered composites are 0.75, 1.3 and 1.48 vol%, which are lower than the nominal content of GPLs within the composites and indicates part of the GPLs is consumed during the high temperature sintering process.

3.1.2 Microstructures of the 'as-prepared' samples

The fracture surfaces of the sintered samples are shown in Figure 2. It can be seen that the pure Al_2O_3 matrix exhibits an intergranular fracture mode while GPL-reinforced Al_2O_3 composites present both an intergranular and intragranular fracture modes. The fracture mode is determined by the strengths of the ceramic matrix and the boundaries between them. For pure Al_2O_3, the strength of grain boundaries are weaker than the Al_2O_3 grains, which enables cracks to propagate along the grain boundaries; while for GPL-reinforced Al_2O_3 composites, the observed fracture mode implies the strengthened grain boundaries and moderate improvement in fracture toughness [27]. Meanwhile, it is noted that GPLs are well distributed in

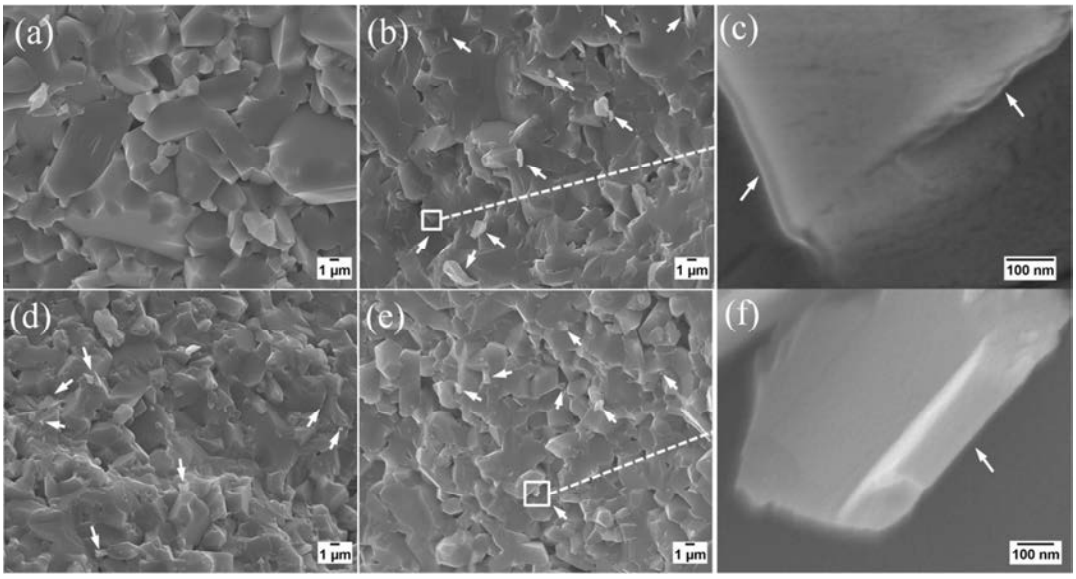

Figure 2. Fracture surfaces of sintered GPL/Al_2O_3 composites. (a) Al_2O_3, (b) 0.75 vol% GPL/Al_2O_3, (d) 1.3 vol% GPL/Al_2O_3, (e) 1.48 vol% GPL/Al_2O_3. (c) and (f) are magnified images of square area in (b) and (e) respectively. White arrows indicate GPLs.

the Al_2O_3 matrices, indicating the good dispersion of GPLs during the ball milling process. In addition, grain sizes of the Al_2O_3 matrices decrease with the increasing percentage of GPLs,

which is attributed to the pinning effect of GPLs in the grain boundaries. To obtain the average grain sizes of the Al_2O_3 matrices, polished and thermally etched surfaces of the sintered samples are characterized using SEM. As shown in Figure 3, significant grain

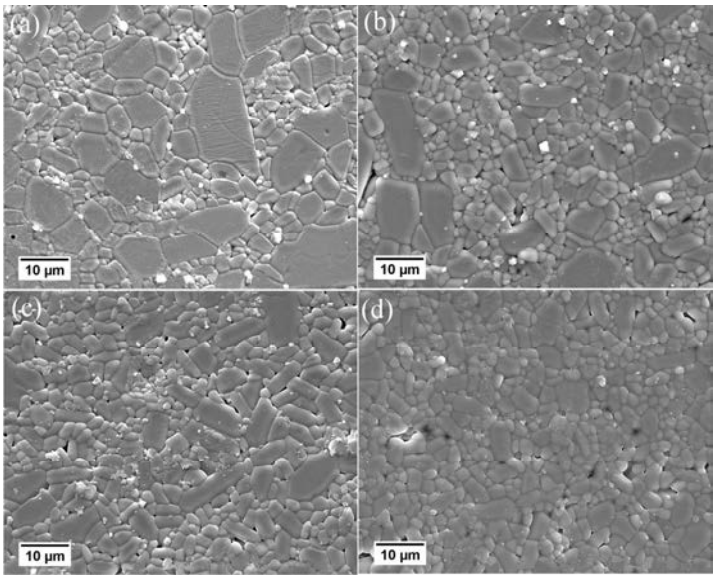

Figure 3. SEM images of polished and thermally etched surfaces. (a) Al_2O_3, (b) 0.75 vol% GPL/Al_2O_3, (c) 1.3 vol% GPL/Al_2O_3, (d) 1.48 vol% GPL/Al_2O_3.

decrease is observed by adding the GPLs. With the increasing percentage of GPLs the Al_2O_3 matrices exhibit a more uniform and finer microstructure. The grain sizes of the Al_2O_3 matrices are plotted in Figure S3. It can be seen that with the increasing concentration of GPLs from 0 to 1.48 vol%, the grain sizes decrease from 4.31 to 2.87 μm. The significant refinement in the matrix microstructure is expected to contribute to the increase in both hardness and flexural strength. The microstructures obtained in present study using 150 nm raw Al_2O_3 particles were compared with those in previous reports with raw Al_2O_3 particle sizes of 140-150 nm [28, 29]. In Santanach's work, the monolithic Al_2O_3 with grain size of 7.5 μm was produced using SPS at 1500 °C [28] while in this work the pure Al_2O_3 prepared at 1650 °C using pressure-less sintering has much smaller grain size. This result implies that the

rate of mass transfer and grain growth in monolithic Al_2O_3 is slower in pressure-less sintering than that in the sintering process with the help of pressure. However, the grain size (2.87 μm) obtained for the 1.4 vol% GPL/Al_2O_3 composite in present study is larger than that (below 1 μm) for the 0.59 vol% GPL/Al_2O_3 composite produced at a lower temperature (1500 °C) using SPS [29]. This fact indicates Al_2O_3 grain growth is more sensitive to the sintering temperature than the GPLs content and the rate of grain growth in GPL/Al_2O_3 composites can be higher in pressure-less sintering than that in pressure sintering due to a relatively higher sintering temperature.

3.1.3 Raman spectra of the pristine GPL and GPLs after ball milling and sintering.

Raman spectra of the pristine GPL and GPLs after the ball milling process are presented in Figure S4. It is very evident that D peaks of GPLs in powder mixtures show pronounced lower intensities than those of the pristine GPL.

To gain further insight into the structures of GPLs Raman parameters are compiled in Table 1. It is noted that GPLs in powder mixtures exhibit much lower ratio of intensities of D to G peaks (I_D/I_G) compared to the pristine GPLs, indicating decreased defects of the GPLs [18]. The result can be explained by agglomeration of GPLs during ball milling, resulting in decreased

Table 1. Raman parameters of the pristine GPL and the GPLs in the powder mixtures

Materials	I_D/I_G	FWHM (G)	ν (G)	FWHM (2D)	ν (2D)	I_{2D}/I_G
Pristine GPL	0.26	20	1582	75	2714	0.65
1.17 vol% GPL/Al_2O_3	0.04	17	1577	75	2712	0.63
1.85 vol% GPL/Al_2O_3	0.06	18	1576	78	2704	0.63
2.75 vol% GPL/Al_2O_3	0.04	18	1571	85	2695	0.52

number of edge defects. On the other hand, the I_{2D}/I_G of the GPLs in powder mixtures is lower than that of the pristine GPL which again indicates the occurrence of an agglomeration of GPLs. In addition, I_{2D}/I_G decreases with the increasing percentage of GPLs, implying addition of a high percentage of GPLs is more prone to causing formation of GPL aggolomerates [22]. This argument can be further supported by the increasing full width at half maximum (FWHM) of 2D bands with an increasing percentage of GPLs.

The Raman spectra of the pristine GPL and GPLs in the sintered samples are compared in Figure 4. It can be seen that GPLs in the sintered samples exhibit much higher spectrum backgrounds compared to the pristine GPL. The increased spectrum backgrounds can be

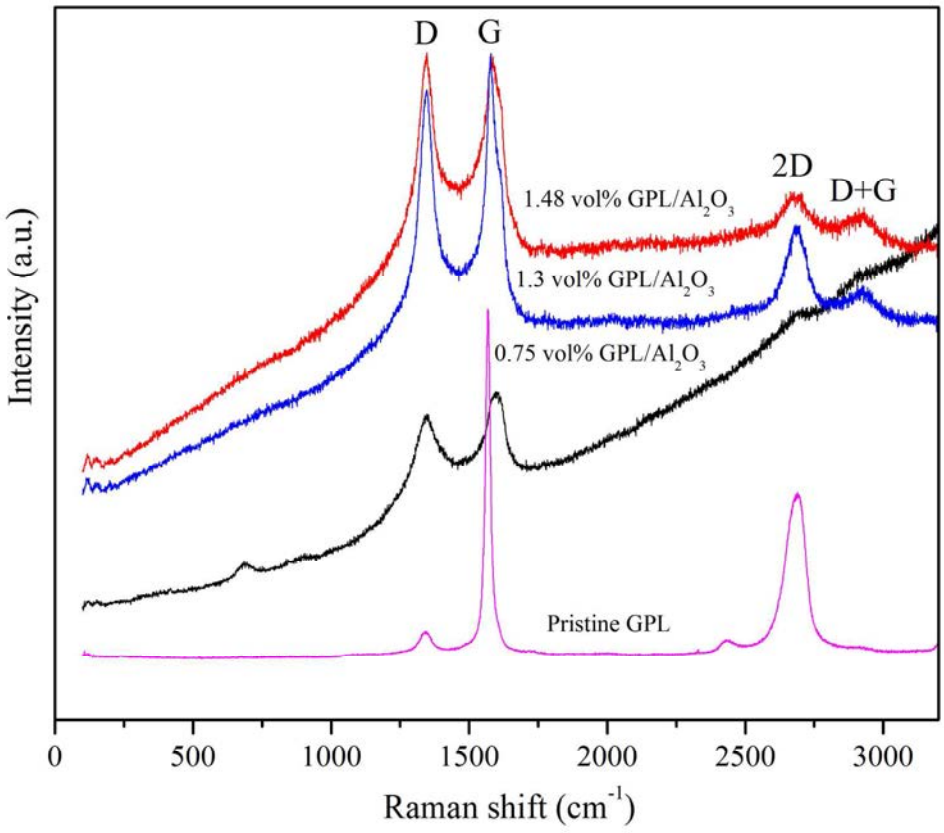

Figure 4. Raman spectra of the pristine GPL and GPLs after sintering.

attributed to interaction of GPLs with the Al_2O_3 during the sintering process. Meanwhile, it is evident that the after sintering GPLs show significantly higher graphitic defects (I_D/I_G) and the presence of D+G mode is observed in sintered samples. On the other hand, it is also noted that GPLs in the sintered samples show far weaker signitures of G and 2D bands in comparision with the pristine GPL, which implies that damage is induced during the sintering process. Similar results were reported in Marc's work where reduced G and 2D peaks were noted after damage was induced in GPLs by a pulsed laser [30]. It has been shown that GPLs can readily absorb the oxygen molecules and hole doping in GPLs by oxygen molecules can take place at a relatively low temperature (300 °C), which would alter the integrity of the GPLs and cause the shift of the G band [31-33]. However, in our work a very high sintering temperature (1650 °C) was used and it is expected that in addition to the hole doping, the interaction between GPLs and oxygen will be significantly enhanced at such a high temperature. As a result, GPLs might be able to react with the oxygen molecules to form gas of carbon dioxide, leading to the loss of the GPLs.

Thinning effect of GPLs due to the interaction between the GPLs and ceramics was suggested in many publications where a SPS furnace was used to consolidate the GPL/ceramic composites in several minutes and at a relatively low sintering temperature (below 1650 °C) [15, 18, 34]. Given the fact that in the present work a much longer sintering time (3 hours) and a relatively higher sintering temperature (1650 °C) were used in sintering process in a flowing inert gas, the interaction between the GPLs and Al_2O_3 would be considerably intensified, causing the consumption of the GPLs. This argument can be indirectly confirmed by the high background of the Raman spectra for GPLs in sintered samples.

The shift of G bands is observed in Figure 4 and are usually attributed to the thermal stress acting on GPLs incurred during thermal contraction of Al_2O_3, increased density of defects in the GPLs and the change in the number of graphene layers [18, 22, 35]. It is worth to note that an

additional factor which can lead to the shifting of the G band is associated with the hole doping, which results from the interaction between the GPLs and oxygen molecules present within the green compacts and the tube [33].

3.1.4 XRD patterns of the pristine GPL and the sintered samples

The XRD analysis of the pristine GPL, pure Al_2O_3 and GPL/Al_2O_3 composites is presented in Figure 5. It can be seen that the GPL exhibits the same XRD pattern as the natural graphite and there is no sign of the presence of new phases in the composites. It is reported that aluminum oxycarbides are likely to be formed during a high temperature sintering process [36]. However, no such phases are observed in the XRD patterns. The reason for this result might be related to the low addition of GPLs which makes it hard to trace the reaction products.

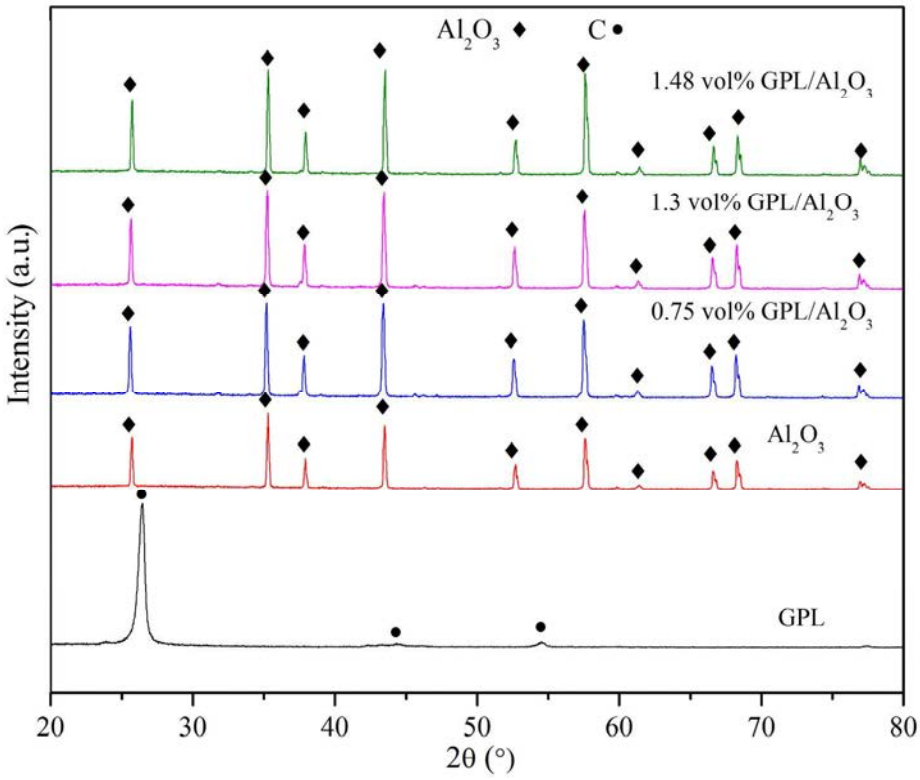

Figure 5. XRD patterns of the pristine GPL, pure Al_2O_3 and GPL/Al_2O_3 composites.

3.1.5 *Mechanical properties of the pressure-less sintered pure Al_2O_3 and GPL/Al_2O_3 composites*

Figure 6a shows the densities of pure Al_2O_3 and GPL/Al_2O_3 composites. It can be seen that the pure Al_2O_3 has been almost fully densified while the GPL-Al_2O_3 composites present relatively lower densities, which decrease from 99.2 to 95.6% with the increasing

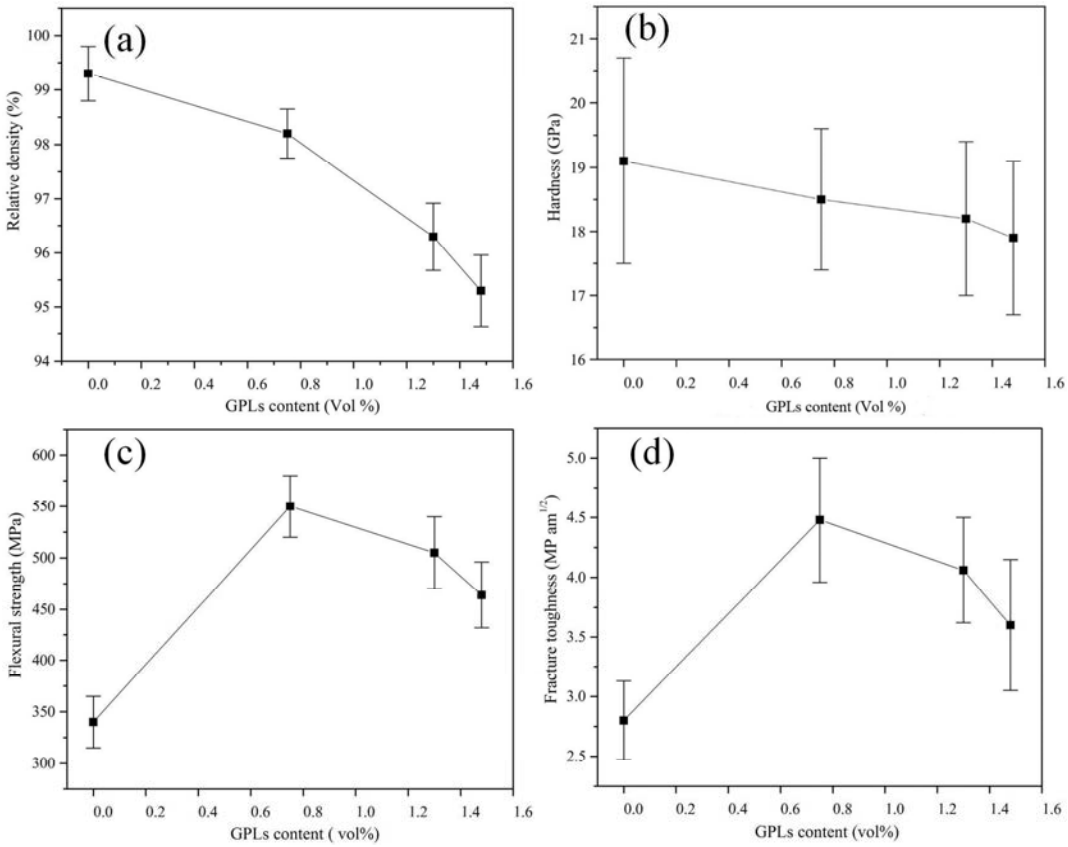

Figure 6. Densities and mechanical properties of the GPL/Al_2O_3 samples as a function of GPLs content.

concentration of GPLs from 0.75 to 1.48 vol%. The result suggests that the addition of GPLs hinders the densifcation process of GPL/Al_2O_3 composites during the pressure-less sintering. In authors' previous work, the 0.76vol% GPL/Al_2O_3 ceramic composite with relative density of 99.92% was successfully fabricated at 1550 °C using SPS within 5 minutes [14] while in

present study the relative density achieved for the 0.75vol% GPL/Al_2O_3 ceramic composite prepared at 1650 °C and in 3 hours was only 98.23%. Therefore, it can be said that the densification rate during the pressure-less sintering is smaller than that in sintering with the aid of pressure and a higher sintering temperature or a longer sintering time may be required to obtain denser GPL/Al_2O_3 samples.

Hardness of pure Al_2O_3 and GPL/Al_2O_3 composites are compared and plotted in Figure 6b. It is noted that the hardness decreases with an increasing percentage of GPLs. Usually higher density and smaller grain size would result in greater hardness. Although the decreased grain size brought by GPLs contributes to the increase of hardness, the lower density of the composites help decrease hardness.

Figure 6c presents flexural strength of the pure Al_2O_3 and GPL/Al_2O_3 composites. It can be observed that the flexural strength of the Al_2O_3 has been significantly improved by adding GPLs and it increases considerably with a minor addition of GPLs and decreases with the further increase of GPLs. A maximum increase of approximately 60% in flexural strength was achieved by introducing 0.75 vol% GPLs. Similar to hardness, flexural strength is mainly affected by the grain size and residual pores. The smaller grain size with reduced flaw size would result in better flexural strength while the presence of pores would allow cracks to be formed easily and cause the small fracture energy due to the stress concentration around the pores [37].

Fracture toughness of the sintered samples is shown in Figure 6d. It is noted that variation in fracture toughness exhibits the same trend as the flexural strength and all of the GPL/Al_2O_3 composites present improved fracture toughness in comparision with pure Al_2O_3. A significant increase in fracture toughness has been achieved by introducing 0.75vol% GPLs. A further increase in GPLs leads to a decrease in fracture toughness. The obtained maxmium

fracture toughness of the GPL/Al_2O_3 composites is appoximately 70% higher than that of pure Al_2O_3.

In this work, the hardness, flexural strength and fracture toughness achieved for the 0.75vol% GPL/Al_2O_3 composite reach 18.58, 550 Mpa and 4.47 Mpa $m^{1/2}$ respectively and are higher than those (17.46, 485 Mpa and 4.11 Mpa $m^{1/2}$) for the 0.76 vol% GPL/Al_2O_3 composite produced using SPS [14]. Therefore, it is expected that pressureles sintering can be able to produce ceramic composites with better mechanical properties than SPS. In particular, given the fact that advanced sintering techniques such as hot pressing and SPS are limited to the fabrication of samples with simple shapes, pressure-less sintering is more advantageous when complex shapes are desired for the sintered samples.

3.1.6 Effects of GPLs on mechanical properties of the GPL/Al_2O_3 composites

As mentioned in previous work [12, 14], the mechanical properties of the densifed GPL-reinforced Al_2O_3 are mainly dependent on the dispersion of GPL in the matrix and interaction between GPLs and the ceramic matrix. In this study, well dispersed GPLs in the ceramic matrix are achieved, as shown in Figures 7 a, c and e. A good dispersion of GPLs in the ceramic matrix would contribute to the mechanical propreties in two ways. On one hand, the distribution of GPLs in the grain boundaries of the ceramic matrix prevents the migration of grain boundaries during the long time sintering process and causes the formation of a fine microstructure, which benefits the flexural strength and fracture toughness by decreasing the defect size of the ceramic matrix and increasing the contact areas between the GPLs and the ceramic matrix respectively. On the other hand, due to the GPLs' high Young's modulus, the embeded GPLs in the ceramic matrix (Figures 7 b, d and f) can reinforce the matrix, leading to improved flexural strength.

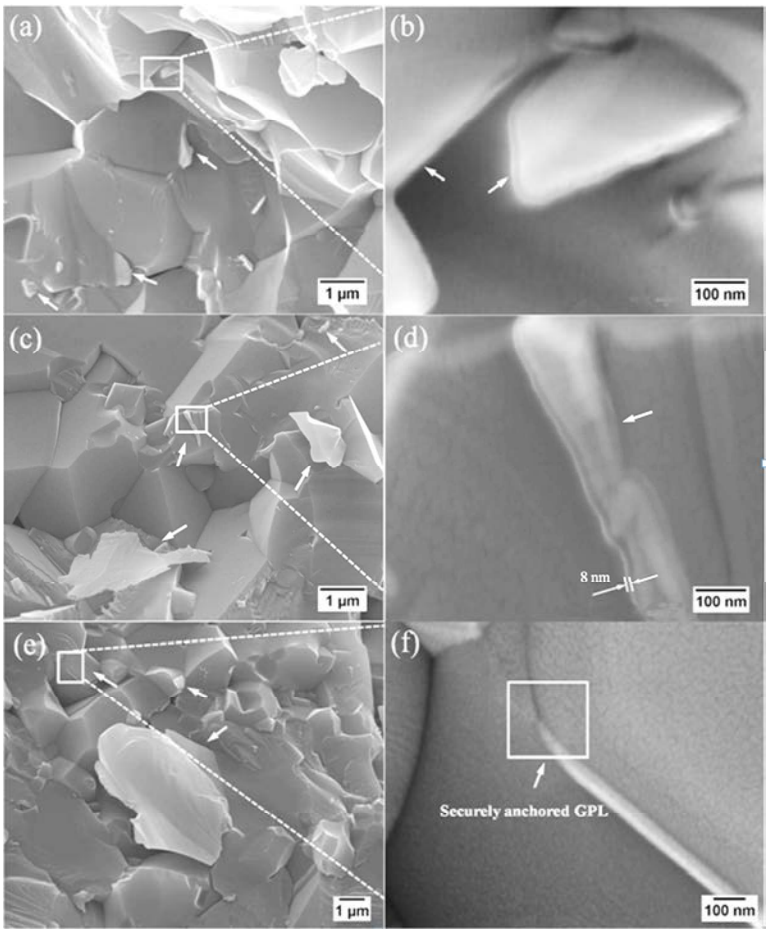

Figure 7. Fracture surfaces of GPL/Al_2O_3 composites. (b), (d) and (f) are the magnified square area in (a), (b) and (e) respectively. White arrows indicate GPLs.

Meanwhile, due to the long sintering time at high temperature, GPLs are securely anchored in the ceramic matrix. Close interaction between GPLs and the ceramic matrix are observed (Figures 7 b and f). A good interaction between GPLs and the ceramic matrix would enable an efficient load transfer from the ceramic matrix to the GPLs, resulting in the improvement in flexural strength. Additionally, high energy is required to overcome the strong interfiacial friction at the interface between the ceramic matrix and the GPLs to pull out the GPLs, leading to the increase in fracture toughness. It should be noted that GPL aggolomerates

(Figures 7 d) are observed and embeded in the ceramic matrix. It is believed that during crack propagation interlayer sliding in the GPL aggolomerates is likely to occur to help energy dissipation and thus contribute to the fracture toughness of the composites [38].

3.2 In-vitro biocompatitability of GPL/Al_2O_3 composites

MTT tests were used to assess cell viability by measuring the levels of active mitochondrial dehydrogenases to convert MTT into formazan crystals. Cell viability of MC3T3 cells on control and sintered samples was investigated with MTT assay after incubation for 3 hours, 1 day and 3days respectively. The results are shown in Figure 8. As expected, the least viability is found for the negative control and the cell viability for the GPL/Al_2O_3 samples is

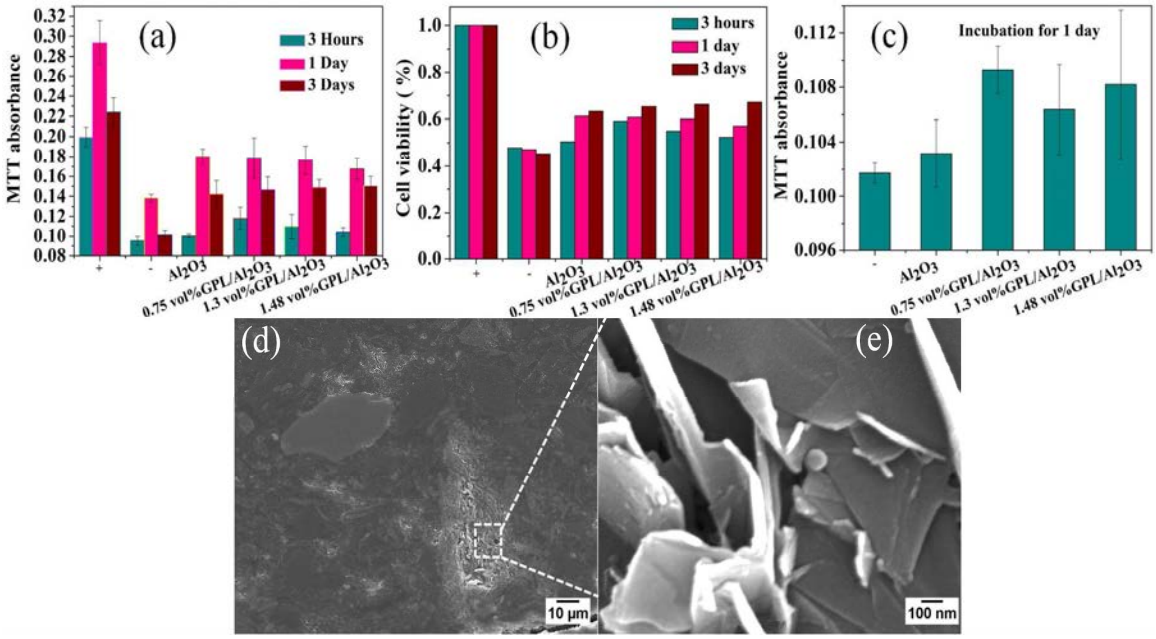

Figure 8. Cell viability on varied samples (a-c) and SEM images of the surfaces of the GPL/Al_2O_3 samples(d-e).

generally higher than that for the monolithic Al_2O_3 after 3 hours or 3 days, which indicates a better initial attachment of cells and viability for GPL/Al_2O_3 samples (Figure 8a and 8b).

However, GPL/Al_2O_3 samples exhibit slightly lower cell viability after 1 day of incubation. Particularly, the 1.48vol% GPLs/Al_2O_3 ceramic composite permits a lower survival rate of cells in comparison to other samples. It implies that during the culturing period, cell proliferated and expanded along the sample surfaces except where the sharp edges of the GPL clusters exposed on the surfaces of the ceramic composites (Figure 8e). These exposed GPL edges prohibit cell proliferation, which causes the decrease in cell survivability on the surfaces. The 1.48 vol% GPLs/Al_2O_3 ceramic composite contains a higher percentage of pores in which more GPLs edges are likely to be exposed on the surface of the ceramic composite. Therefore, lower cell viability was found for the 1.48vol% GPLs/Al_2O_3 ceramic composite.

Another parallel set of MTT tests were carried out using DMEM without addition of fetal bovine serum, to investigate initial cell adhesion on substrates without the disturbance of serum proteins (Figure 8c). The result suggests that more cells attached on GPL/Al_2O_3 samples as compared to the monolithic Al_2O_3 sample after incubation for 1 day. These results show that the GPL/Al_2O_3 ceramic has comparable or more favourable biocompatibility for osteoblast precursor cells, which is in agreement with the reported work concerning the graphene reinforced HA composites [22].

Cell adhesion tests were also performed using BMSCs and the florescence images are shown in Figure 9. It can be observed that cells with different morphologies are present on the materials. The number of the cells is reduced with the addition of GPLs. This observation indicates negative effect of GPL on the proliferation of stem cells. However, as suggested by Figure 9c-e, cells on the surfaces of the GPL/Al_2O_3 composites demonstrate better elongation and expansion. This might indicate that the presence of GPLs stimulated adhered BMSCs in a way that growing and expanding is encouraged while cell division is prohibited. The mixed

results suggest that other factors such as surface morphology [7], porosity, contact angle with cell media and surface chemistry [8], accumulation of charge [9] and the grain size of the ceramics might also play an important role in the interaction between stem cells and material surfaces. Other tests need to be done in the future to examine the complex behaviour of stem cells on the composite, for example cell differentiation identification.

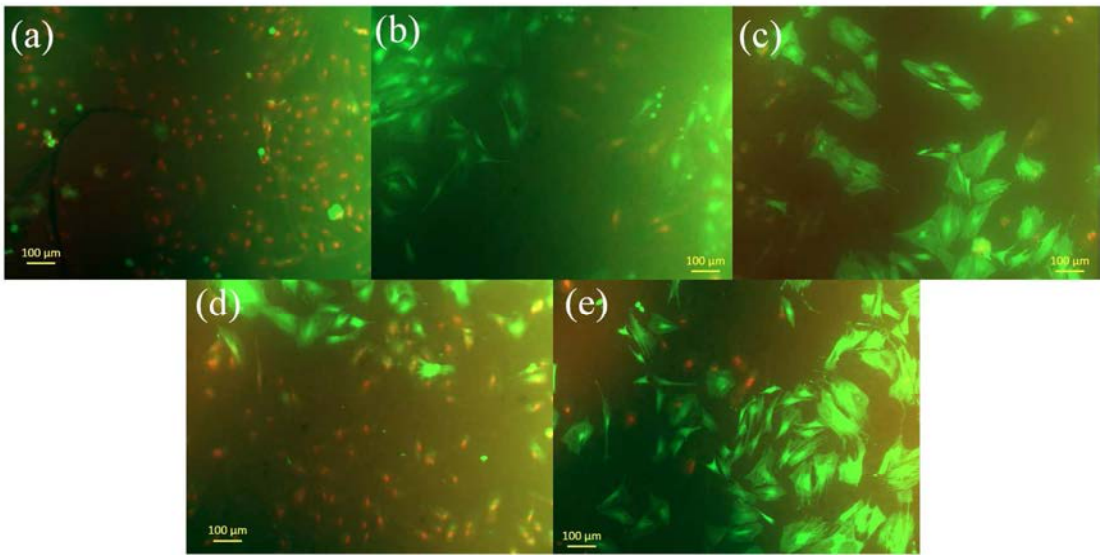

Figure 9. Fluorescence microscopy images of the stem cells on the PDMS (a), Al_2O_3 (b), 0.75 vol% GPL/Al_2O_3 (c), 1.3 vol% GPL/Al_2O_3 (d) ,1.48 vol% GPL/Al_2O_3 (e).

The survival rate of the cells was qualitatively calculated and shown in Figure S5 based upon the observed results shown in Figure 9. It is found that the number of attached cells and adherent live cells for the GPL/Al_2O_3 composites is smaller than that for monolithic Al_2O_3 (Figure S5a), indicating un-preferable attachment of stem cells on the GPL/Al_2O_3 composites. However, the survival rate of the stem cells on composites with additions of 0.75 and 1.48vol% GPLs are noticed to be higher than that on the monolithic Al_2O_3 (Figure S5b). It is believed that the variation in the survivability of the stem cells (Figure S5b) can be explained by the double effects of the GPL content and the pores within the ceramics. The presence of pores

will increase the likelihood of GPL edges being exposed to the cells, leading to the death of the cells (Figure 8e) while the GPLs with flat surfaces can certainly facilitate the spread and proliferation of the cells.

Previous reports have shown that both CNT/Al_2O_3 composites produced by HIP [2] and GPL/HA composites fabricated using SPS [22] exhibit attractive biocompabilities and cell viability has been increased due to the addition of carbon fillers. Similar results were obtained in this study using pressure-less sintering. In particular, the enhanced spread of stem cells on the GPL/Al_2O_3 composites observed in the study is promising for the materials to be used in a variety of biomedical purposes in the future and pressure-less sintering can certainly be a possible means to produce such materials.

4. Conclusions

In the study, GPL/Al_2O_3 composites were successfully fabricated using a pressure-less sintering process. A minor addition of GPLs has demonstrated to be able to efficiently improve the fracture toughness as well as flexural strength of the Al_2O_3 ceramics. The pull-out toughening mechanism and strong interaction between the GPLs and the matrix are regarded as the reasons for the improvements. XRD and Raman results suggest that no traceable reaction products in the GPL/Al_2O_3 composites were found after the sintering and graphitic defects in GPLs were produced during the high temperature processing. MTT tests show that the GPL/Al_2O_3 ceramic has comparable or more favourable biocompatibility toward osteoblasts. However, the cell adhesion tests with stem cells indicate otherwise, possibly caused by the pores and GPL edges exposed to the cells, leading to the narcosis of the cells while the GPLs with flat surfaces can facilitate the spread and proliferation of the cells. Other factors affecting the interaction between the stem cells and ceramics can be

surface morphology, porosity, contact angle with cell media and surface chemistry, accumulation of charge and the grain size of the ceramics.

Supporting information

SEM images of the powder mixtures, TGA of the sintered samples, Grain sizes of GPL/Al_2O_3 composites, Raman spectra of the pristine GPL and GPLs in powder mixtures and living and dead BMSCs after culturing for 3 Days. The material is available free of charge via the Internet at http://pubs.acs.org.

Acknowledgment

This publication is based on the research supported by the European Horizon 2020 under grant number 644971, 111 Programme under grant number B12016 and Innovative UK project under grant number 710705.

References

1. Boutin, P.; Christel, P.; Dorlot, J. M.; Meunier, A.; de Roquancourt, A.; Blanquaert, D.; Herman, S.; Sedel, L.; Witvoet, J., The Use of Dense Alumina–Alumina Ceramic Combination in Total Hip Replacement. *J. Biomed. Mater. Res.* **1988,** *22* (12), 1203-1232.

2. Ogihara, N.; Usui, Y.; Aoki, K.; Shimizu, M.; Narita, N.; Hara, K.; Nakamura, K.; Ishigaki, N.; Takanashi, S.; Okamoto, M.; Kato, H.; Haniu, H.; Ogiwara, N.; Nakayama, N.; Taruta, S.; Saito, N., Biocompatibility and Bone Tissue Compatibility of Alumina Ceramics Reinforced with Carbon Nanotubes. *Nanomed.* **2012,** *7* (7), 981-993.

3. Ueda, K.; Oba, S.; Omiya, Y.; Okada, M., Cranial-Bone Defects with Depression Deformity Treated with Ceramic Implants and Free-Flap Transfers. *Br. J. Plast. Surg.* **2001,** *54* (5), 403-408.

4. Wang, J.K.; Lai, P.C.; Liao, S. L., Late Exposure of the Bioceramic Orbital Implant. *Am. J. Ophthalmol.* **2009,** *147* (1), 162-170.

5. Raigrodski, A. J.; Chiche, G. J.; Potiket, N.; Hochstedler, J. L.; Mohamed, S. E.; Billiot, S.; Mercante, D. E., The Efficacy of Posterior Three-Unit Zirconium-Oxide–Based Ceramic Fixed Partial Dental Prostheses: A Prospective Clinical Pilot Study. *J. Prosthet. Dent.* **2006,** *96* (4), 237-244.

6. Pirker, W.; Kocher, A., Immediate, Non-submerged, Root-Analogue Zirconia Implants Placed into Single-Rooted Extraction Sockets: 2-Year Follow-up of a Clinical Study. *Int. J. Oral. Maxillofac. Surg.* **2009,** *38* (11), 1127-1132.

7. Palmero, P.; Fornabaio, M.; Montanaro, L.; Reveron, H.; Esnouf, C.; Chevalier, J., Towards Long Lasting Zirconia-Based Composites for Dental Implants. Part I: Innovative Synthesis, Microstructural Characterization and In Vitro Stability. *Biomaterials* **2015,** *50* (0), 38-46.

8. Becher, P. F.; Sun, E. Y.; Plucknett, K. P.; Alexander, K. B.; Hsueh, C.-H.; Lin, H.-T.; Waters, S. B.; Westmoreland, C. G.; Kang, E.-S.; Hirao, K.; Brito, M. E., Microstructural Design of Silicon Nitride with Improved Fracture Toughness: I, Effects of Grain Shape and Size. *J. Am. Ceram. Soc.* **1998,** *81* (11), 2821-2830.

9. Rajendran, S., Production of Ultrafine Alpha Alumina Powders and Fabrication of Fine Grained Strong Ceramics. *J. Mater.Sci.* **1994,** *29* (21), 5664-5672.

10. Zhan, G. D.; Mitomo, M.; Kim, Y.-W., Microstructural Control for Strengthening of Silicon Carbide Ceramics. *J. Am. Ceram. Soc.* **1999,** *82* (10), 2924-2926.

11. Geim, A. K.; Novoselov, K. S., The Rise of Graphene. *Nat. Mater.* **2007,** *6* (3), 183-191.

12. Liu, J.; Yan, H.; Reece, M. J.; Jiang, K., Toughening of Zirconia/Alumina Composites by the Addition of Graphene Platelets. *J. Euro. Ceram. Soc.* **2012,** *32* (16), 4185-4193.

13. Frank, I. W.; Tanenbaum, D. M.; van der Zande, A. M.; McEuen, P. L., Mechanical Properties of Suspended Graphene Sheets. *J. Vac. Sci. Technol.B.* **2007,** *25* (6), 2558-2561.

14. Liu, J.; Yan, H.; Jiang, K., Mechanical Properties of Graphene Platelet-Reinforced Alumina Ceramic Composites. *Ceram. Int.* **2013,** *39* (6), 6215-6221.

15. Porwal, H.; Tatarko, P.; Grasso, S.; Khaliq, J.; Dlouhy, I.; Reece, M. J., Graphene Reinforced Alumina Nano-Composites. *Carbon* **2013,** *64*, 359-369.

16. Walker, L. S.; Marotto, V. R.; Rafiee, M. A.; Koratkar, N.; Corral, E. L., Toughening in Graphene Ceramic Composites. *ACS Nano* **2011,** *5* (4), 3182-3190.

17. Dusza, J.; Morgiel, J.; Duszová, A.; Kvetková, L.; Nosko, M.; Kun, P.; Balázsi, C., Microstructure and Fracture Toughness of Si3N4+Graphene Platelet Composites. *J. Euro. Ceram. Soc.* **2012,** *32* (12), 3389-3397.

18. Yadhukulakrishnan, G. B.; Karumuri, S.; Rahman, A.; Singh, R. P.; Kaan Kalkan, A.; Harimkar, S. P., Spark Plasma Sintering of Graphene Reinforced Zirconium Diboride Ultra-High Temperature Ceramic Composites. *Ceram. Int.* **2013,** *39* (6), 6637-6646.

19. Nieto, A.; Lahiri, D.; Agarwal, A., Graphene NanoPlatelets Reinforced Tantalum Carbide Consolidated by Spark Plasma Sintering. *Mater. Sci. Eng. A.* **2013,** *582* (0), 338-346.

20. Liu, S.; Zeng, T. H.; Hofmann, M.; Burcombe, E.; Wei, J.; Jiang, R.; Kong, J.; Chen, Y., Antibacterial Activity of Graphite, Graphite Oxide, Graphene Oxide, and Reduced Graphene Oxide: Membrane and Oxidative Stress. *ACS Nano* **2011,** *5* (9), 6971-6980.

21. Zhang, Y.; Ali, S. F.; Dervishi, E.; Xu, Y.; Li, Z.; Casciano, D.; Biris, A. S., Cytotoxicity Effects of Graphene and Single-Wall Carbon Nanotubes in Neural Phaeochromocytoma-Derived PC12 Cells. *ACS Nano* **2010,** *4* (6), 3181-3186.

22. Zhang, L.; Liu, W.; Yue, C.; Zhang, T.; Li, P.; Xing, Z.; Chen, Y., A Tough Graphene Nanosheet/Hydroxyapatite Composite with Improved In Vitro Biocompatibility. *Carbon* **2013,** *61* (0), 105-115.

23. Lahiri, D.; Dua, R.; Zhang, C.; de Socarraz-Novoa, I.; Bhat, A.; Ramaswamy, S.; Agarwal, A., Graphene Nanoplatelet-Induced Strengthening of UltraHigh Molecular Weight Polyethylene and Biocompatibility In vitro. *ACS Appl. Mater. Inter.* **2012,** *4* (4), 2234-2241.

24. Hsiao, M. C.; Liao, S. H.; Yen, M. Y.; Liu, P. I.; Pu, N. W.; Wang, C. A.; Ma, C. C. M., Preparation of Covalently Functionalized Graphene Using Residual Oxygen-Containing Functional Groups. *ACS Appl. Mater. Inter.* **2010,** *2* (11), 3092-3099.

25. Fan, Y.; Zhang, X.; Liu, Y.; Cai, Q.; Zhang, J., One-pot Hydrothermal Synthesis of Mn3O4/Graphene Nanocomposite for Supercapacitors. *Mater. Lett.* **2013,** *95*, 153-156.

26. Hwang, J. Y.; El-Kady, M. F.; Wang, Y.; Wang, L.; Shao, Y.; Marsh, K.; Ko, J. M.; Kaner, R. B., Direct Preparation and Processing of Graphene/RuO2 Nanocomposite Electrodes for High-Performance Capacitive Energy Storage. *Nano Energy* **2015,** *18*, 57-70.

27. Awaji, H.; Choi, S. M.; Yagi, E., Mechanisms of Toughening and Strengthening in Ceramic-Based Nanocomposites. *Mech. Mater.* **2002,** *34* (7), 411-422.

28. Santanach, J. G.; Weibel, A.; Estournes, C.; Yang, Q.; Laurent, C.; Peigney, A., Spark Plasma Sintering of Alumina: Study of Parameters, Formal Sintering Analysis and Hypotheses on the Mechanisms Involved in Densification and Grain growth. *Acta Mater.* **2011,** *59* (4), 1400-1408.

29. Centeno, A.; Rocha, V. G.; Alonso, B.; Fernandez, A.; Gutierrez-Gonzalez, C. F.; Torrecillas, R.; Zurutuza, A., Graphene for Tough and Electroconductive Alumina Ceramics. *J. Euro. Ceram. Soc.* **2013,** *33* (15-16), 3201-3210.

30. Currie, M.; Caldwell, J. D.; Bezares, F. J.; Robinson, J.; Anderson, T.; Chun, H. D.; Tadjer, M., Quantifying Pulsed Laser Induced Damage to Graphene. *Appl. Phys. Lett.* **2011,** *99* (21).

31. Liu, W. J.; Tran, X. A.; Liu, X. B.; Wei, J.; Yu, H. Y.; Sun, X. W., Characteristics of a Single-Layer Graphene Field Effect Transistor with UV/Ozone Treatment. *Ecs Solid State Lett.* **2013,** *2* (1), M1-M4.

32. Yang, Y.; Murali, R., Binding Mechanisms of Molecular Oxygen and Moisture to Graphene. *Appl. Phys. Lett.* **2011,** *98* (9), 093116.

33. Ryu, S.; Liu, L.; Berciaud, S.; Yu, Y.-J.; Liu, H.; Kim, P.; Flynn, G. W.; Brus, L. E., Atmospheric Oxygen Binding and Hole Doping in Deformed Graphene on a SiO2 Substrate. *Nano Lett.* **2010,** *10* (12), 4944-4951.

34. Liu, J.; Li, Z.; Yan, H. X.; Jiang, K. L., Spark Plasma Sintering of Alumina Composites with Graphene Platelets and Silicon Carbide Nanoparticles. *Adv. Eng. Mater.* **2014,** *16* (9), 1111-1118.

35. Ni, Z. H.; Wang, H. M.; Ma, Y.; Kasim, J.; Wu, Y. H.; Shen, Z. X., Tunable Stress and Controlled Thickness Modification in Graphene by Annealing. *ACS Nano* **2008,** *2* (5), 1033-1039.

36. Sarkar, S.; Das, P. K., Statistical Analysis of Mechanical Properties of Pressureless Sintered Multiwalled Carbon Nanotube/Alumina Nanocomposites. *Mater. Chem. Phys.* **2012,** *137* (2), 511-518.

37. Ahmad, K.; Pan, W.; Qu, Z. X., Multifunctional Properties of Alumina Composites Reinforced by a Hybrid Filler. *Int. J. Appl. Ceram. Tec.* **2009,** *6* (1), 80-88.

38. Nieto, A.; Lahiri, D.; Agarwal, A., Synthesis and Properties of Bulk Graphene Nanoplatelets Consolidated by Spark Plasma Sintering. *Carbon* **2012,** *50* (11), 4068-4077.

Table of Contents

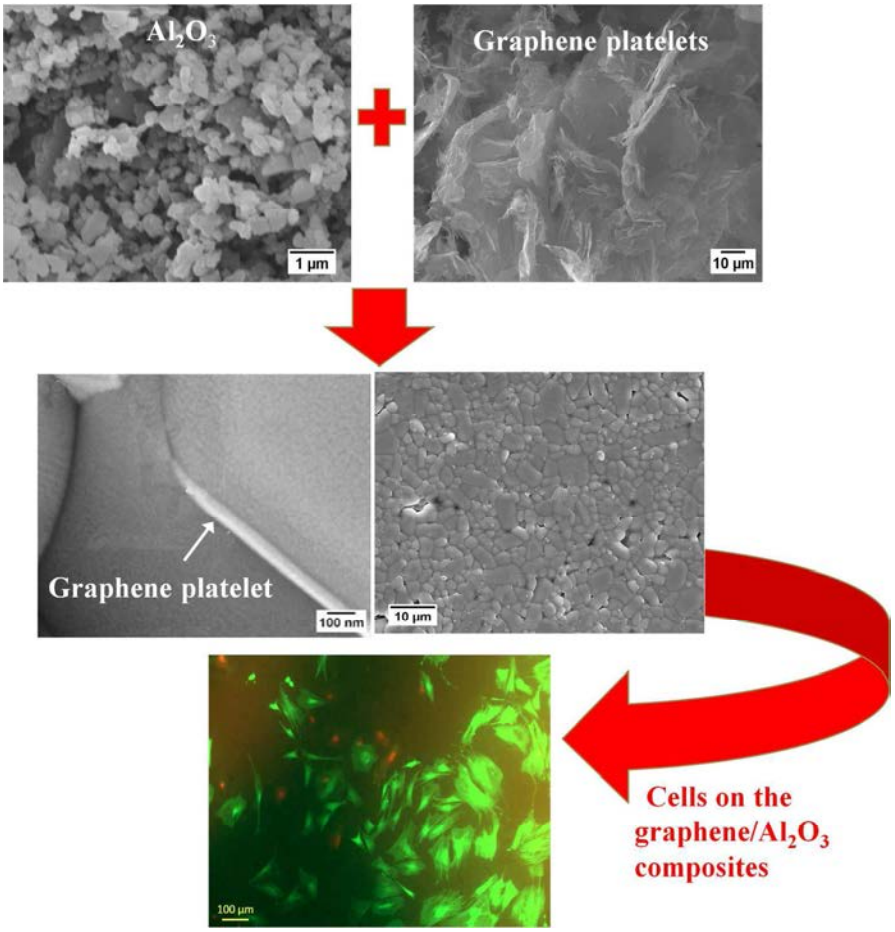

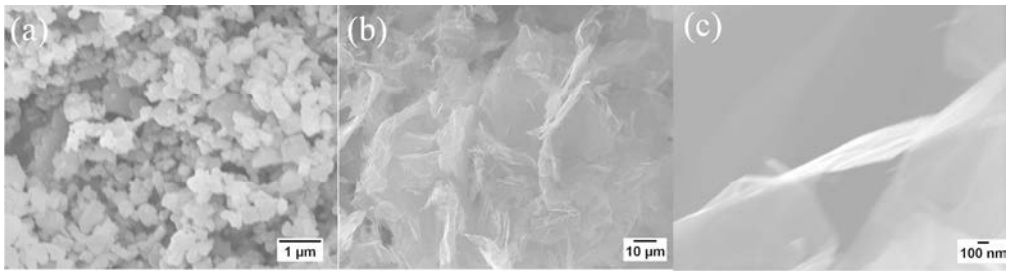

Figure.1 SEM images of Al2O3 (a) powders and GPLs (b-c).
453x120mm (300 x 300 DPI)

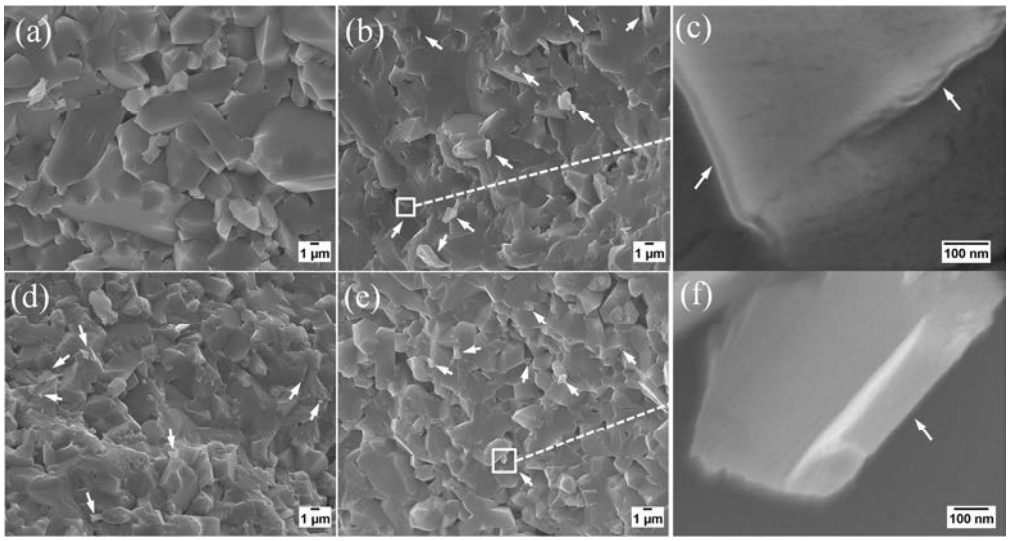

Figure 2. Fracture surfaces of sintered GPL/Al2O3 composites. (a) Al2O3, (b) 0.75 vol% GPL/Al2O3, (d) 1.3 vol% GPL/Al2O3, (e) 1.48 vol% GPL/Al2O3. (c) and (f) are magnified images of square area in (b) and (e) respectively. White arrows indicate GPLs.
376x200mm (150 x 150 DPI)

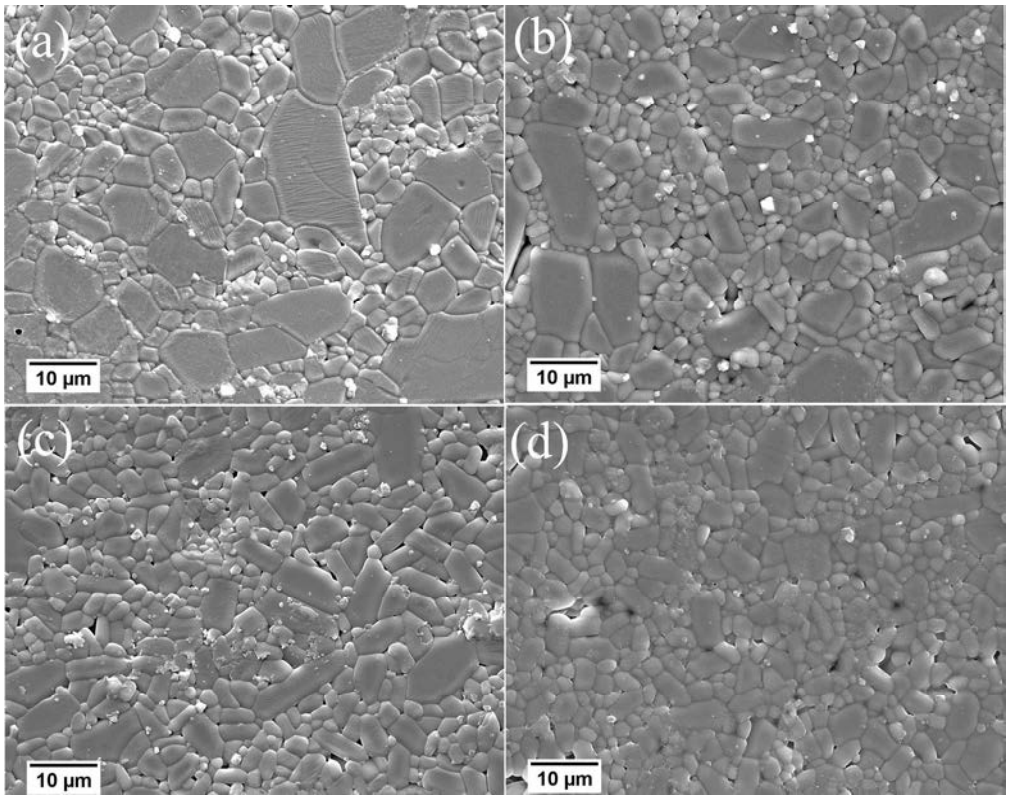

Figure 3. SEM images of polished and thermally etched surfaces. (a) Al2O3, (b) 0.75 vol% GPL/Al2O3, (c) 1.3 vol% GPL/Al2O3, (d) 1.48 vol% GPL/Al2O3.
326x257mm (150 x 150 DPI)

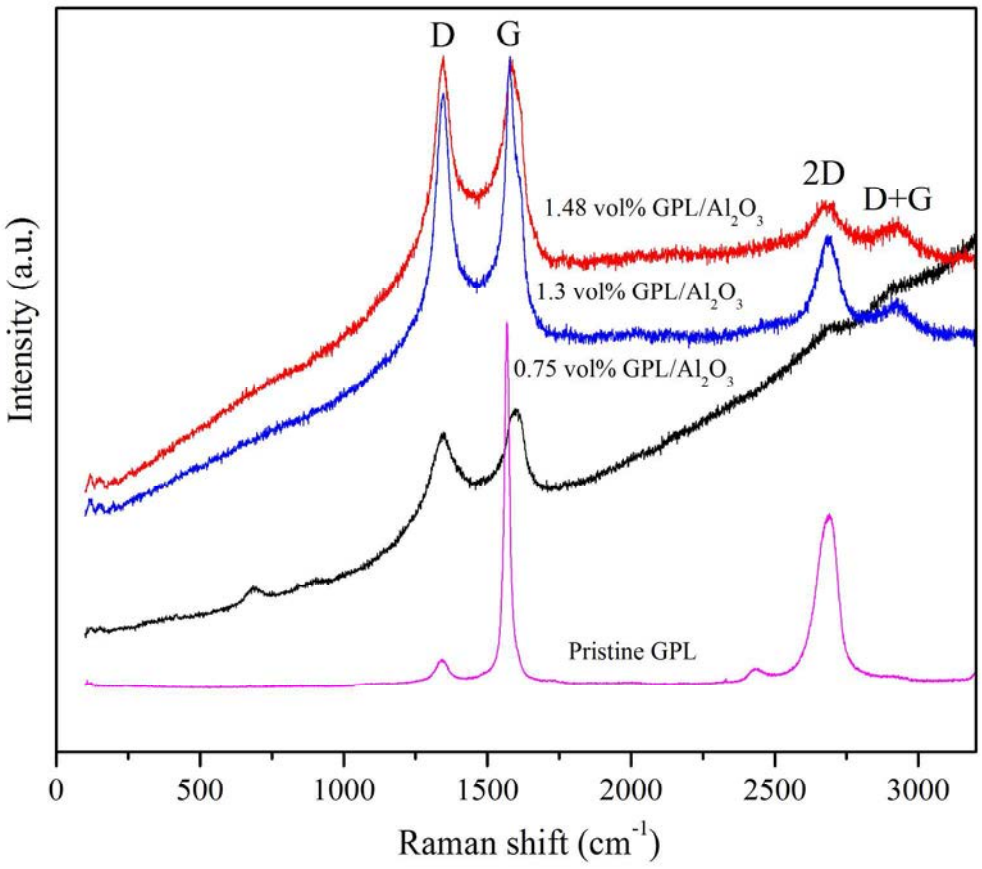

Figure 4. Raman spectra of the pristine GPL and GPLs after sintering.
202x180mm (300 x 300 DPI)

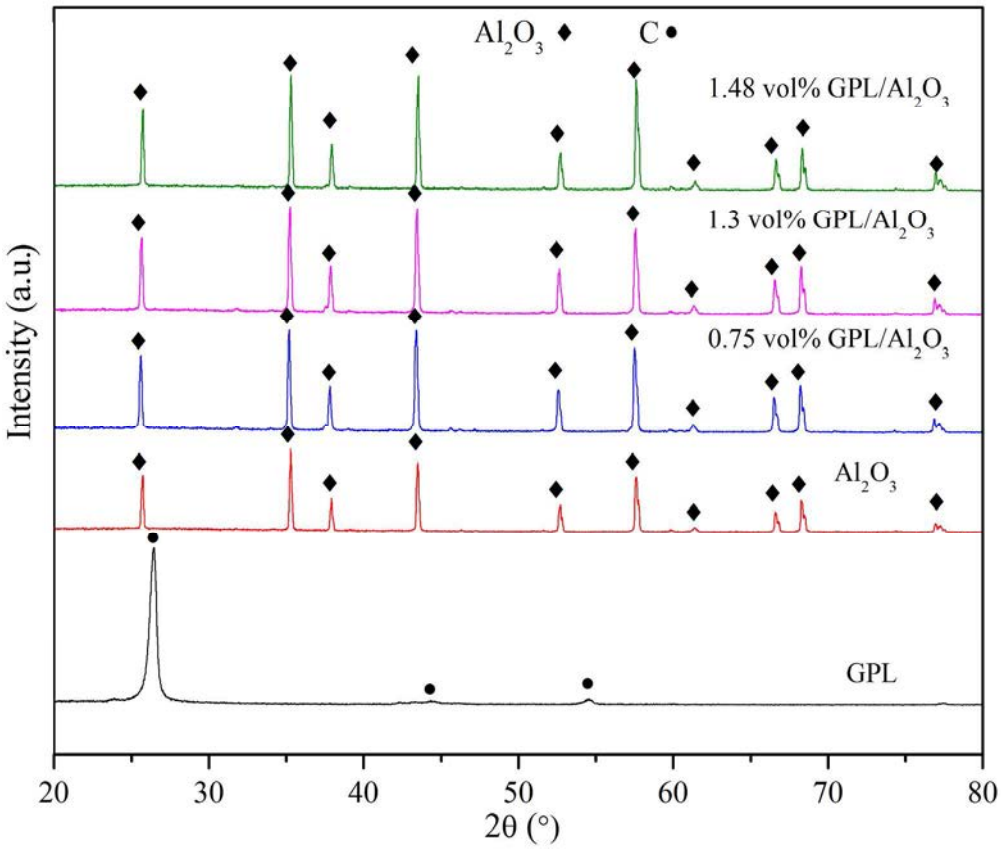

Figure 5. XRD patterns of the pristine GPL, pure Al2O3 and GPL/Al2O3 composites.
209x178mm (300 x 300 DPI)

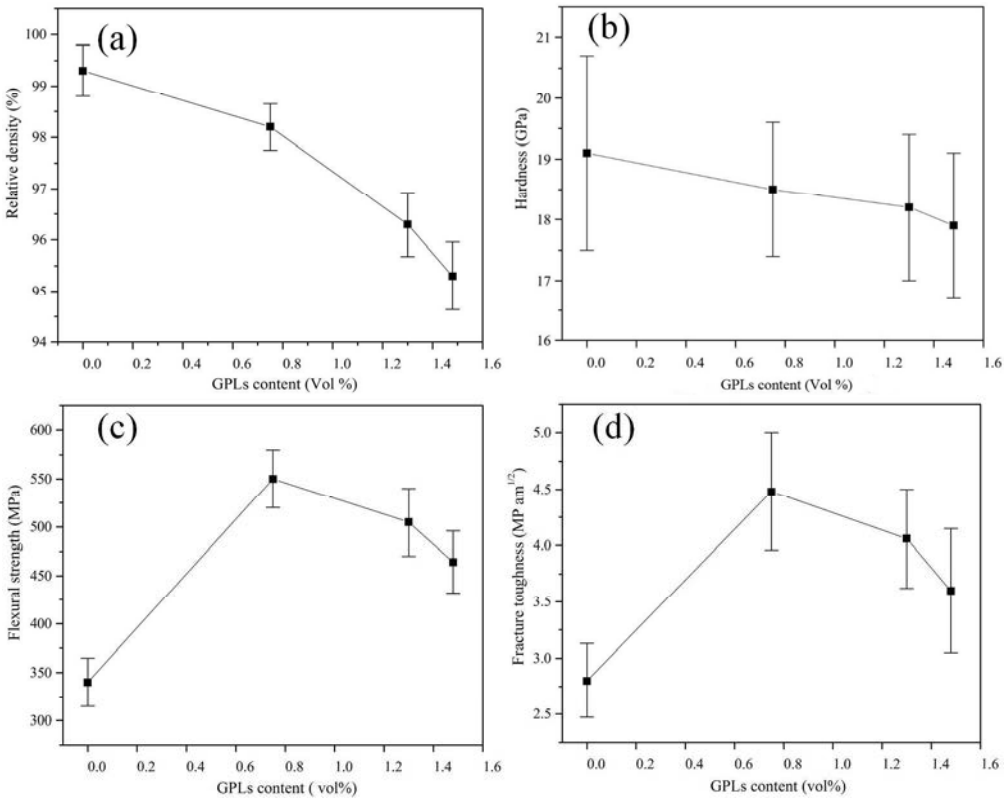

Figure 6. Densities and mechanical properties of the GPL/Al2O3 samples as a function of GPLs content.
428x344mm (150 x 150 DPI)

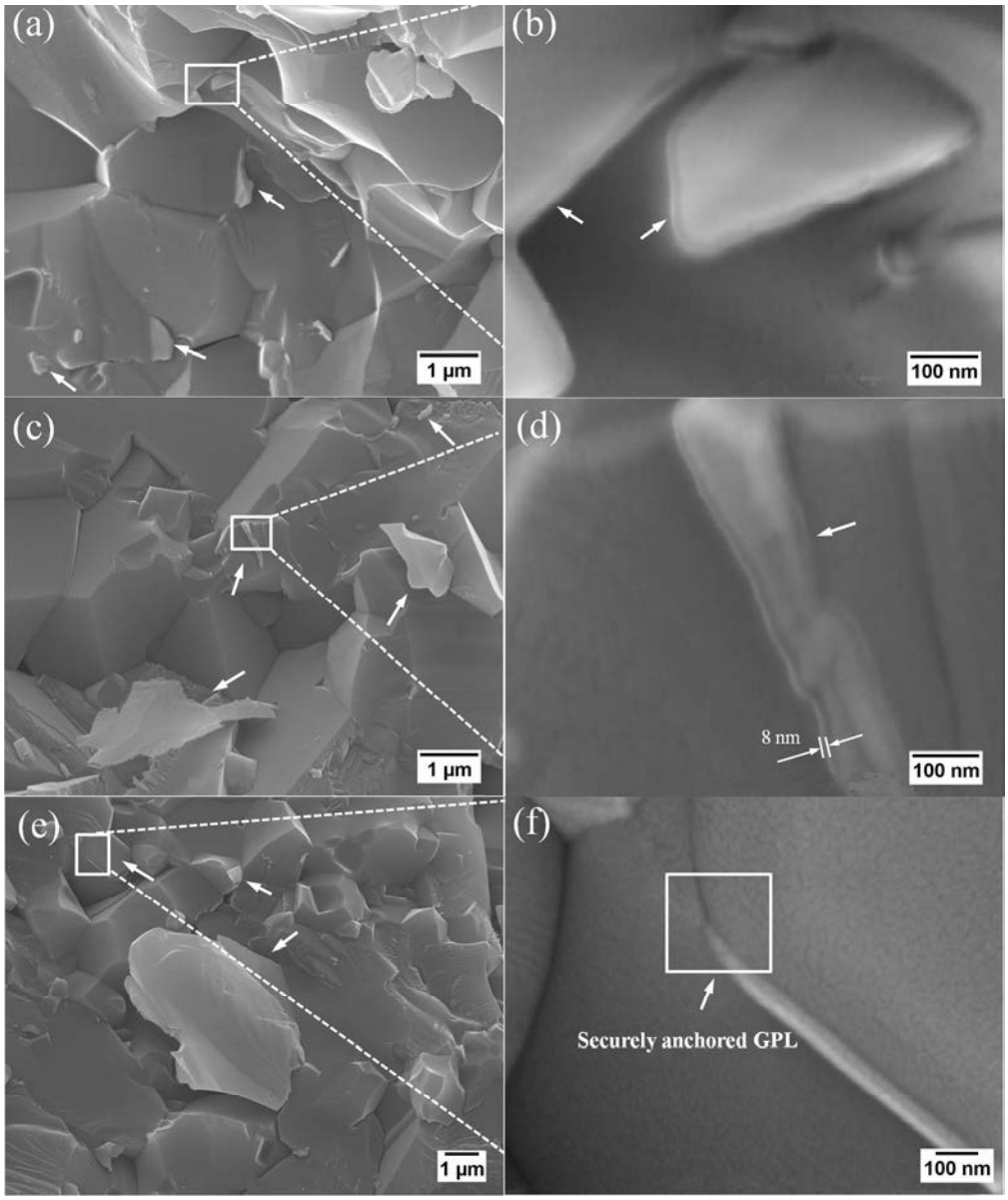

Figure 7. Fracture surfaces of GPL/Al2O3 composites. (b), (d) and (f) are the magnified square area in (a), (b) and (e) respectively. White arrows indicate GPLs.
326x388mm (150 x 150 DPI)

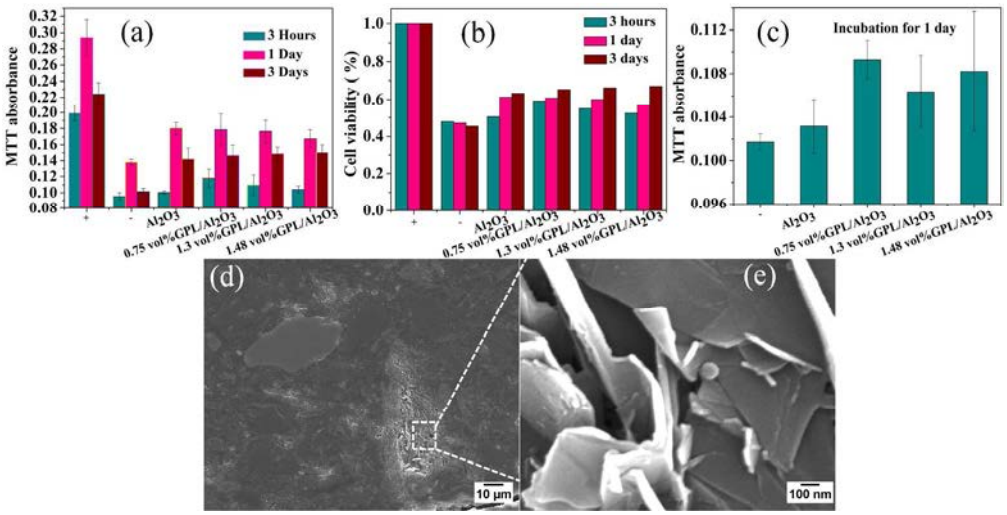

Figure 8. Cell viability on varied samples (a-c) and SEM images of the surfaces of the GPL/Al2O3 samples(d-e).
476x241mm (150 x 150 DPI)

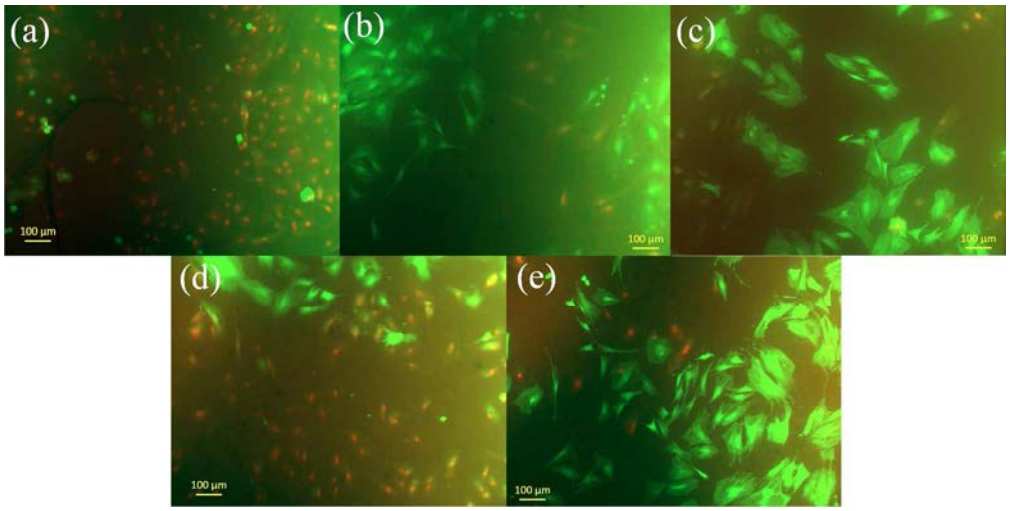

Figure 9. Fluorescence microscopy images of the stem cells on the PDMS (a), Al2O3 (b), 0.75 vol% GPL/Al2O3 (c), 1.3 vol% GPL/Al2O3 (d) ,1.48 vol% GPL/Al2O3 (e).
439x219mm (150 x 150 DPI)

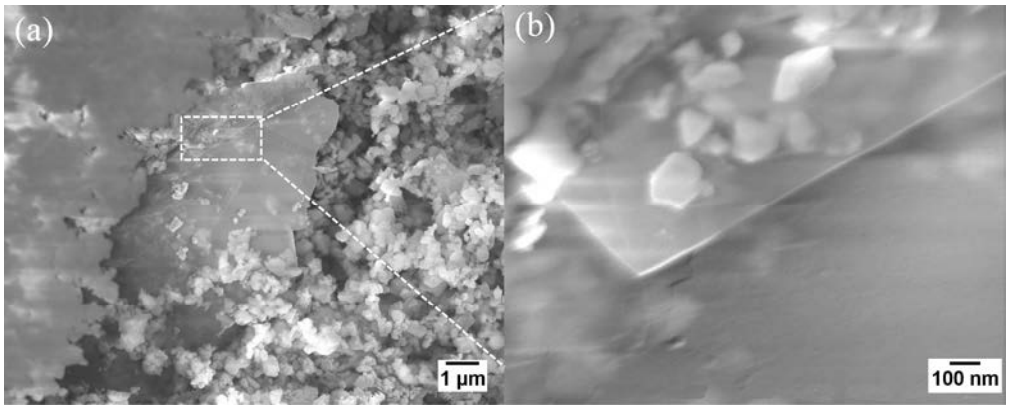

Figure S1. SEM images of the powder mixtures. (b) is the magnified square area in (a), showing GPL.
449x179mm (300 x 300 DPI)

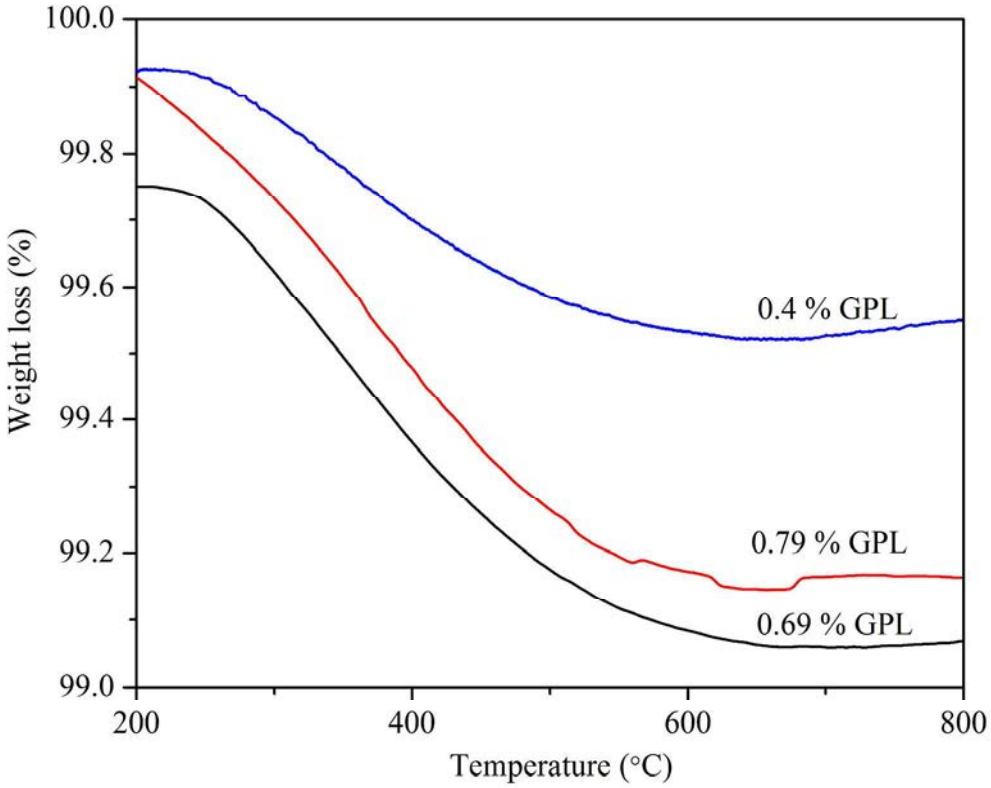

Figure S2. TGA of the sintered samples with different GPLs content.
225x181mm (300 x 300 DPI)

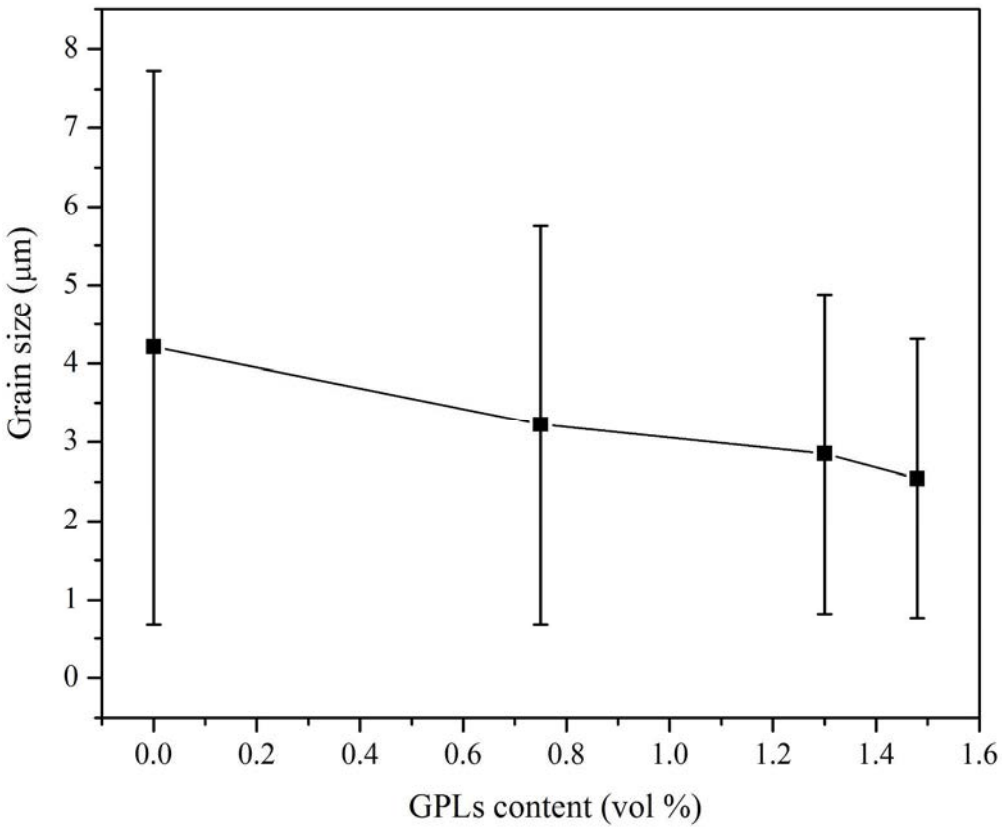

Figure S3. Grain sizes of Al2O3 matrices as a function of content of GPLs.
212x176mm (300 x 300 DPI)

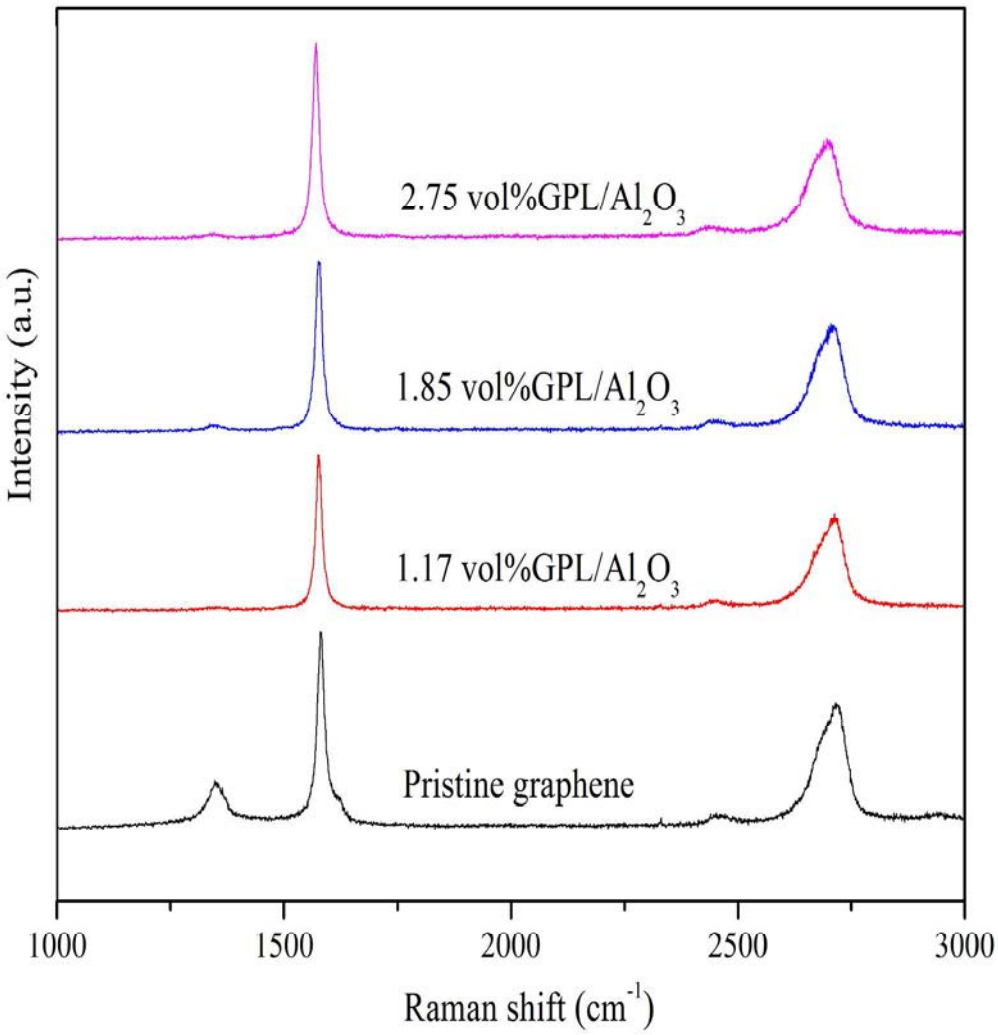

Figure S4. Raman spectra of the pristine GPL and GPLs in powder mixtures.
215x224mm (300 x 300 DPI)

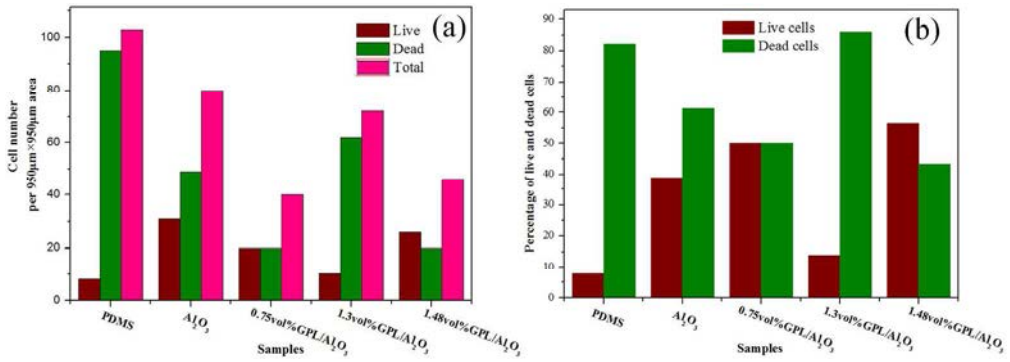

Figure S5. Living and dead BMSCs in a 950 um×950 um area after culturing for 3 Days. (a) and (b) show the cell number and percentage of live and dead cells on the samples respectively.
507x180mm (300 x 300 DPI)